Quantifying functional phenotypes in human pluripotent stem cell derived cardiomyocytes for disease modelling and drug discovery

Meer, B.J. van

Abstract

There are several methods to measure cardiomyocyte (CM) and muscle contraction but these require customized hardware, expensive apparatus and advanced informatics or can only be used in single experimental models. Consequently, data and techniques have been difficult to reproduce across models and laboratories, analysis is time consuming and only specialist researchers can quantify data. Here we describe and validate an automated, open source software tool (MUSCLEMOTION) adaptable for use with standard laboratory- and clinical imaging equipment that enables quantitative analysis of normal cardiac contraction, disease phenotypes and pharmacological responses. MUSCLEMOTION allowed rapid and easy measurement of movement from high-speed movies in: (i) 1-dimensional *in vitro* models such as isolated adult and human pluripotent stem cell-derived CMs (hPSC-CMs); (ii) 2-dimensional *in vitro* models, such as beating CM monolayers or small clusters of hPSC-CMs; (iii) 3-dimensional multicellular *in vitro* or *in vivo* contractile tissues such as cardiac "organoids", engineered heart tissues (EHT), zebrafish- and human hearts. MUSCLEMOTION was effective under different recording conditions (bright field microscopy with simultaneous patch clamp recording, phase contrast microscopy and traction force microscopy). Outcomes were virtually identical to the current gold standards for contraction measurement such as optical flow, pole deflection, edge-detection systems or manual analyses. Finally, we used the algorithm to quantify contraction in *in vitro* and *in vivo* arrhythmia models and to measure pharmacological responses. Using a single open source method for processing video recordings, we obtained reliable pharmacological data and measures of cardiac disease phenotype in experimental cell-, animal- and human models.

Chapter 3

MUSCLEMOTION: a versatile open software tool to quantify cardiomyocyte and cardiac muscle contraction *in vitro* and *in vivo*

Modified after Circulation Research 122, e5-e16 (2018)

Berend van Meer#, Luca Sala#, Leon Tertoolen, Jeroen Bakkers, Milena Bellin, Richard Davis, Chris Denning, Michel Dieben, Thomas Eschenhagen, Elisa Giacomelli, Catarina Grandela, Arne Hansen, Eduard Holman, Monique Jongbloed, Sarah Kamel, Lotte Koopman, Quintin Lachaud, Ingra Mannhardt, Mervyn Mol, Diego Mosqueira, Valeria Orlova, Robert Passier, Marcelo Ribeiro, Umber Saleem, Godfrey Smith*, Francis Burton*, Christine Mummery*

# these authors contributed equally to this work
* these authors contributed equally to this work

Introduction

The salient feature of cardiomyocytes (CMs) is their ability to undergo cyclic contraction and relaxation, a feature critical for cardiac function. In many research laboratories and clinical settings it is therefore essential that cardiac contraction can be quantified at multiple levels, from single cells to multicellular or intact cardiac tissues. Measurement of contractility is relevant for analysis of disease phenotypes, cardiac safety pharmacology, and longitudinal measures of cardiac function over time, both *in vitro* and *in vivo*. In addition, human genotype-phenotype correlations, investigation of cardiac disease mechanisms and the assessment of cardiotoxicity are increasingly performed on human induced pluripotent stem cells (hiPSCs) derived from patients[1-3]. Many of these studies are carried out in non-specialist laboratories so that it is important that analysis methods are simplified such that they can be used anywhere with access to just standard imaging equipment. Here, we describe a single method with high versatility that can be applied to most imaging outputs of cardiac contraction likely to be encountered in the laboratory or clinic.

Electrical and calcium signals are usually quantified *in vitro* using established technologies such as patch clamp electrophysiology, multi electrode arrays (MEAs), cation-sensitive dyes or cation-sensitive genetic reporters[4]. Although experimental details differ among laboratories, the values for these parameters are with some approximations comparable across laboratories, cardiomyocyte source and cell culture configuration (e.g. single cells, multicellular 2-Dimensional (2D) CM monolayers, 3-Dimensional (3D) cultures)[5,6]. However, there is no comparable method for measuring cardiac contraction across multiple platforms, despite this being a crucial functional parameter affected by many diseases or drugs[7]. We have developed a method to address this that is built on existing algorithms and is fully automated, but most importantly can be used on videos, image stacks or image sequences loaded in the open source image processing program ImageJ[8]. Moreover, it is an open source, dynamic platform that can be expanded, improved and integrated for customized applications. The method, called MUSCLEMOTION, determines dynamic changes in pixel intensity between image frames and expresses the output as a relative measure of movement during muscle contraction and relaxation. We applied the concept to a range of biomedical- and pharmacologically relevant experimental models that included single hPSC-CMs, patterned- or 2D cultures of hPSC-CMs, cardiac organoids, engineered heart tissues (EHTs) and isolated adult rabbit CMs. Results were validated by comparing outputs of the tool with those from three established methods for measuring contraction: optical flow, post deflection and fractional shortening of sarcomere length. These methods have been tailored to (or only work on) specific cell configurations. Traction force microscopy, fractional shortening of sarcomere length and microposts are predominantly suitable for single cells[8,9]. Cardiomyocyte edge or perimeter detection is suitable for adult CMs but challenging for immature hPSC-CMs due to poorly defined plasma membrane borders and concentric contraction[10], while large post deflection is suitable for EHTs or small cardiac bundles[11] but less so for single cells. Our MUSCLEMOTION software by contrast can be used for all of these applications without significant adaptions. Furthermore, it can be used for multi-parameter recording conditions and experimental settings using transmitted light microscopy, fluorescent membrane labeling, fluorescent beads

embedded in soft substrates or patch clamp video recordings. Drug responses to positive and negative inotropic agents were evaluated across four different laboratories in multiple cell configurations using MUSCLEMOTION with reliable predictions of drug effects from all laboratories. Furthermore, MUSCLEMOTION was also applicable to optical recordings of zebrafish hearts *in vivo*, where it represented a significant time-saving in analysis, and in human echocardiograms. This versatile tool thus provides a rapid and straightforward way to detect disease phenotypes and pharmacological responses *in vitro* and *in vivo.*

Results

Algorithm development

The principle underlying the algorithm of MUSCLEMOTION is the assessment of contraction using an intuitive approach quantifying absolute changes in pixel intensity between a reference frame and the frame of interest, which can be described as

$$|img_i - img_{ref}| = img_{result}$$

where is the frame of interest, is the reference frame and is the resulting image. For every pixel in the frame, each reference pixel is subtracted from the corresponding pixel of interest and the difference is presented in absolute numbers. Unchanged pixels result in low (black) values, while pixels that are highly changed result in high (white) values (Figure 1a). Next, the mean pixel intensity of the resulting image is measured. This is a quantitative measure of how much the pixels have moved compared to the reference frame: more white pixels indicate more changing pixels and, thus, more displacement. When a series of images is analysed relative to the same reference image, the output describes the accumulated displacement over time (measure of displacement, Figure 1b).

However, if a series of images is analysed with a reference frame that depends on the frame of interest (e.g. $img_{ref} = img_{i-1}$), this results in a measure of the relative displacement per interframe interval. We defined this parameter as contraction velocity (measure of velocity, Figure 1b).

Since velocity is the first derivative of displacement in time, the first derivative of the measure of displacement should resemble the measure of velocity derived from image calculations. To test the linearity of the method, three movies of moving blocks were analysed. The block moved back and forth at two different speeds in each direction (where): i) along the x-axis, ii) along the y-axis and iii) along both axes (Supplementary Movie 1). As expected, the measure of displacement and velocity showed a linear correlation (Supplementary Figure 1). This does not hold when the position of the block in does not overlap the position of the block in , with a consequent saturation in the measure of displacement (i.e. max pixel white value, Supplementary Figure 2). Therefore, comparison of the differentially derived velocities should approximately overlap in the absence of pixel saturation. This was used as a qualitative parameter to determine whether the algorithm outputs were reliable.

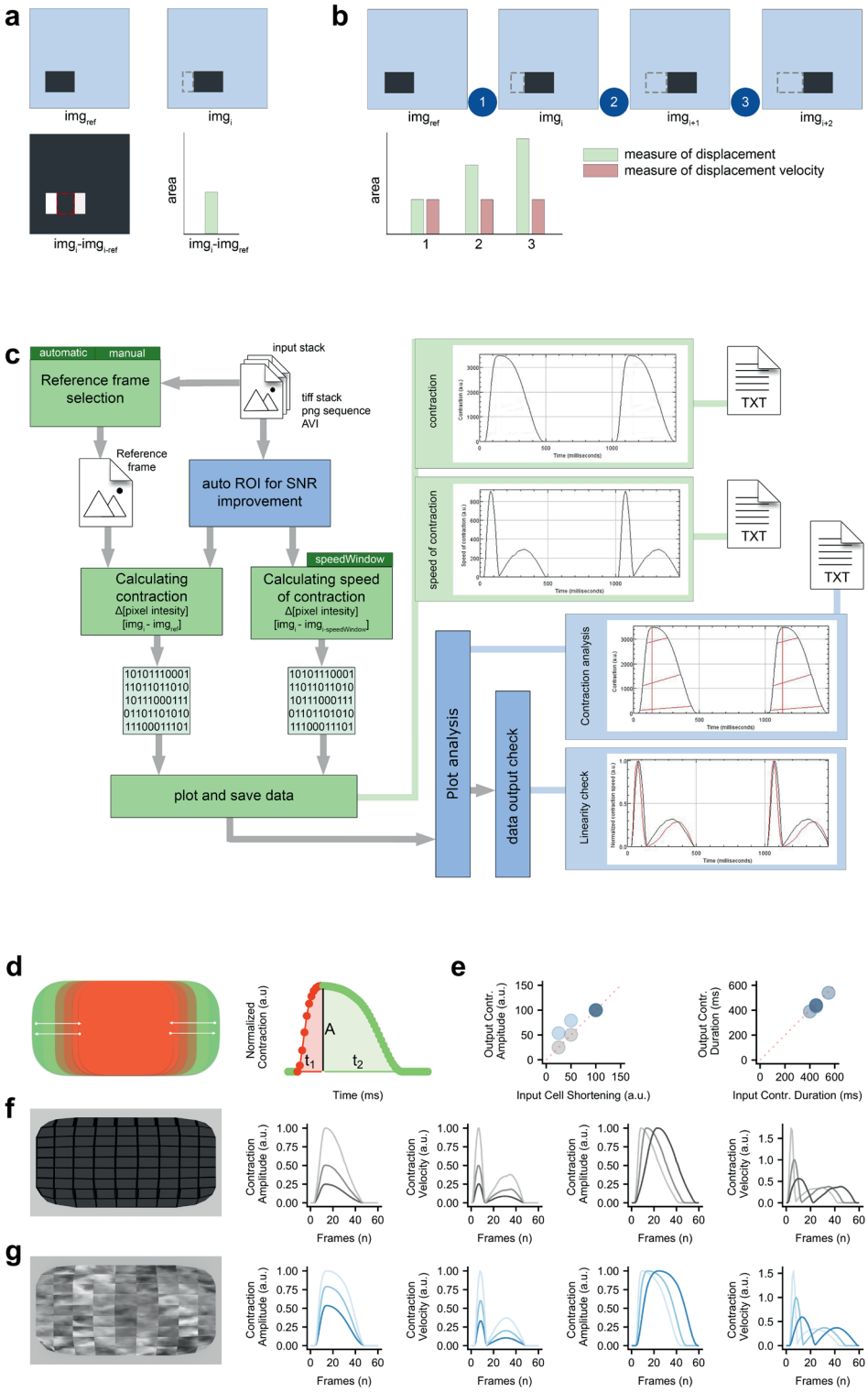
a
b
c
d
e
f
g
measure of displacement
measure of displacement velocity
automatic
manual
Reference frame selection
input stack
tiff stack
png sequence
AVI
Reference frame
auto ROI for SNR improvement
speedWindow
Calculating contraction
Δ[pixel intesity]
Calculating speed of contraction
Δ[pixel intesity]
plot and save data
contraction
speed of contraction
TXT
Plot analysis
data output check
Contraction analysis
Linearity check
Normalized Contraction (a.u)
Time (ms)
Output Contr. Amplitude (a.u.)
Input Cell Shortening (a.u.)
Output Contr. Duration (ms)
Input Contr. Duration (ms)
Contraction Amplitude (a.u.)
Contraction Velocity (a.u.)
Frames (n)

Algorithm implementation

MUSCLEMOTION was then modified to handle typical experimental recordings by (i) improving the signal-to-noise ratio (SNR), (ii) automating reference frame selection and (iii) programming built-in checks to validate the generated output data (Figure 1c). The SNR was increased by isolating the pixels of interest in a three-step process: i) maximum projection of pixel intensity in the complete contraction stack, ii) creation of a binary image of this maximum projection with a threshold level equal to the mean grey value plus standard deviation and iii) multiplication of the pixel values in this image by the original contraction and speed of the contraction image stack (Supplementary Figure 3). This process allowed the algorithm to work on a region of interest with movement above the noise level only.

Next, a method was developed to identify the correct from the speed of contraction image stack by comparing values obtained from the frame-to-frame calculation with their direct neighbouring values, while also checking for the lowest absolute value (Supplementary Figure 4).

The reliability of MUSCLEMOTION for structures with complex movements was validated using a custom-made contracting 3D "synthetic CM" model (Figure 1d,f,g) that was adapted to produce contractions with known amplitude and duration. Linearity was preserved during the analysis of the contraction and velocity; other output parameters of the analysis matched the input parameters (Figure 1e). A second 3D model (Figure 1g), with a repetitive pattern aimed to create out-of-bounds problems was also generated. As expected, contraction amplitude information here was not linear (Figure 1e), although contraction velocity and temporal parameters did remain linear (Figure 1e,g). To mitigate this problem, we implemented an option for a 10-sigma

Figure 1: Algorithm construction and validation.

a) Principle of pixel intensity difference by subtraction of imgref of imgi and measurement of the non-zero area after image subtraction. b) Principle of using pixel intensity difference as a measure of displacement and as a measure of displacement velocity. c) Schematic overview of MUSCLEMOTION. Green blocks indicate basic steps of the algorithm. Dark green blocks indicate important user input choices. Plots within light green blocks indicate results. Optional steps are shown in blue blocks, with graphical representation of the analysed parameters indicated by red lines. Three result files are generated containing the raw data: "contraction.txt", "speed-of-contraction.txt" and "overview-results.txt". Furthermore, three images showing relevant traces and a log file are generated and saved (not shown in schematic). d) Schematic of the contractile pattern of the artificial cell and relative parameters corresponding to amplitude of contraction (A), time-to-peak (t1) and relaxation time (t2). e) Correlation between input (x axis) and output (y axis) parameters used to validate MUSCLEMOTION with two artificial cells. f-g) Frame representing the two artificial cells built for MUSCLEMOTION validation and their relative output parameters.

Gaussian blur filter that can be applied on demand to biological samples that presented highly repetitive patterns (e.g. sarcomeres in adult CMs).

Algorithm application to multiple cell configurations and correlation with existing gold standards

This set of experiments aimed to investigate the versatility of MUSCLEMOTION and examine how its performance compared with standard measures used in each system: i) optical flow for isolated hPSC-CMs, monolayers and organoids; ii) post deflection for EHT; iii) sarcomere length fractional shortening for adult CMs. Remarkably, standard methods currently used measure only contraction or contraction velocity. Linearity was preserved in all cases during the analyses, demonstrating the reliability of the results (Supplementary Figure 5).

First, single hPSC-CMs (Figure 2a, Supplementary Movie 2) exhibited concentric contraction (Figure 2a ii) and contraction velocity amplitudes correlated well with the amplitudes obtained by optical flow analysis ($R^2 = 0.916$) (Figure 2a v). In contrast to single cells, the area of contraction for hPSC-CM monolayers was distributed heterogeneously throughout the whole field (Figure 2b ii, Supplementary Movie 3). Optical flow analysis was compared with our measure of velocity (Figure 2b iv); this showed a good linear correlation ($R^2 = 0.803$) (Figure 2b v). Complex (mixed, multicellular) 3D configurations were also investigated by analyzing hPSC-derived cardiac organoids[18] (Supplementary Movie 4) and EHTs[15] (Supplementary Movie 5). Cardiac organoids showed moderate levels of contraction throughout the tissue (Figure 2c ii), while the EHTs showed high deflection throughout the bundle (Figure 2d ii). The contraction velocity of the organoids correlated well with the output of optical flow analysis ($R^2 = 0.747$, Figure 2c v). Similarly, contraction amplitudes in EHTs showed high linear correlation ($R^2 = 0.879$) with the absolute force values derived from measurement of pole deflection (Figure 2d v). Finally, single adult rabbit ventricular CMs were analyzed (Figure 2e, Supplementary Movie 6). Large movement was evident around the long edges of the CM (Figure 2e ii). These cells were analyzed with a 10-sigma Gaussian blur filter, which also minimized (unwanted) effects of transverse movements on contraction patterns. Linearity was preserved (Supplementary Figure 5) despite the repetitive pattern of the sarcomeres and this resulted in accurate measures of both contraction (Figure 2e iii) and speed of contraction (Figure 2e iv). The contraction amplitude of the adult CMs stimulated at 1 Hz correlated well with the output of sarcomeric shortening using fast Fourier transform analysis[23] ($R^2 = 0.871$, Figure 2e v). Thus, the MUSCLEMOTION algorithm yielded data in these initial studies comparable with methods of analysis tailored for the individual platforms.

Application of MUSCLEMOTION to multiple imaging and recording platforms

To examine whether MUSCLEMOTION could potentially be used in applications that measure other aspects of CMs functionality in parallel, we first determined the electrophysiological properties of hPSC-CMs using patch clamp whilst recording their contractile properties through video imaging. This allowed simultaneous quantitative measurement of action potentials (APs) and contraction (Figure 3a), for in-depth investigation of their interdependence. We observed a typical[24] profile of AP followed by its delayed contraction.

To measure contractile force in combination with contractile velocity in single CMs, we integrated fluorescent beads into polyacrylamide substrates patterned with gelatin (Figure 3b), where the displacement of the beads is a measure of CM contractile force[20] (Supplementary Movie 7). Additionally, field potentials and contraction profiles of hPSC-CMs were analyzed from simultaneous electrical and video recordings of monolayers plated on MEAs (Figure 3c, Supplementary Movie 8).

Similarly, effective quantification of contraction profiles was obtained for fluorescently labeled hPSC-CM monolayer cultures (Figure 3d, Supplementary Movie 9), allowing MUSCLEMOTION to be integrated on high speed fluorescent microscope systems for automated data analysis.

Application of MUSCLEMOTION to drug responses in different cell models in different laboratories

Having shown that MUSCLEMOTION was fit-for-purpose in analyzing contraction over a variety of platforms, we next sought to demonstrate its ability to detect the effects of positive and negative inotropes. This is essential for ensuring the scalability of the tool over multiple platforms, particularly in the context of hiPSC-CMs where regulatory authorities and pharmaceutical companies are interested in using these cells as human heart models for drug discovery, target validation or safety pharmacology[25]. For isoprenaline (ISO) and nifedipine (NIFE) the main parameters of interest are: contraction amplitude (ISO, NIFE), relaxation time (ISO) and contraction duration (NIFE).

The relaxation time of spontaneously beating isolated hPSC-CMs on gelatin patterned polyacrylamide substrates treated with ISO significantly decreased as expected at doses higher than 1 nM. Similar to what has been reported[27], contraction amplitude decreased at doses higher than 1 nM. NIFE treatment decreased both contraction amplitude and duration starting from 3 nM, respectively (Figure 4a). In paced (1.5 Hz) hPSC-CMs monolayers, no significant effects were measured after addition of ISO on either relaxation time or contraction amplitude. NIFE caused a progressive decrease in contraction duration and amplitude in a concentration-dependent manner starting at 100 nM (Figure 4b). Similarly, cardiac organoids paced at 1.5 Hz showed no significant effects on both relaxation time and contraction amplitude with ISO, while both parameters decreased after NIFE, starting from 100 nM and 300 nM, respectively (Figure 4c). EHTs paced at 1.5 times baseline frequency and analyzed with MUSCLEMOTION showed a positive inotropic effect starting from 1 nM ISO and a negative inotropic effect starting at 30 nM NIFE as previously reported[15] (Figure 4d).

Paced (1 Hz) adult rabbit CMs exhibited no significant increase in relaxation time and contraction amplitude at any ISO concentration. At concentrations higher than 3 nM, adult CMs exhibited after-contractions and triggered activity during diastole, which hampered their ability to be paced at a fixed frequency. No significant effects were observed on contraction duration with NIFE, while contraction amplitude significantly decreased in a dose-dependent manner starting from 100 nM (Figure 4e). Data generated by post deflection and sarcomere fractional shortening are available for comparison purposes in Supplementary Figure 6.

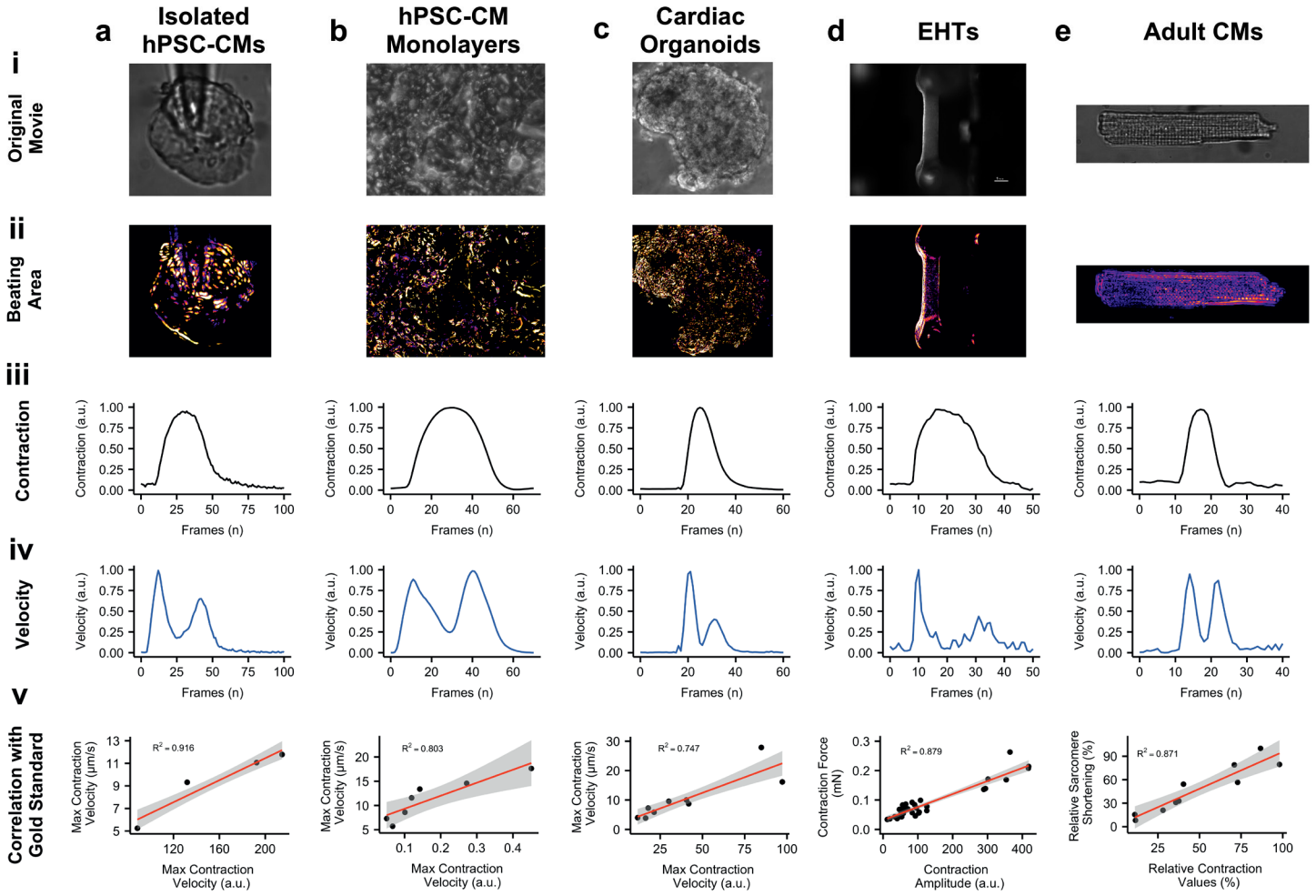
a Isolated hPSC-CMs
b hPSC-CM Monolayers
c Cardiac Organoids
d EHTs
e Adult CMs
i Original Movie
ii Beating Area
iii Contraction
iv Velocity
v Correlation with Gold Standard
Contraction (a.u.)
Velocity (a.u.)
Frames (n)
Max Contraction Velocity (µm/s)
Max Contraction Velocity (a.u.)
Contraction Force (mN)
Contraction Amplitude (a.u.)
Relative Sarcomere Shortening (%)
Relative Contraction Values (%)
R² = 0.916
R² = 0.803
R² = 0.747
R² = 0.879
R² = 0.871

Analysis of disease phenotypes *in vitro*

Contractility of hiPSC-CMs carrying mutations associated with Long QT Syndrome Type 1 (LQT1)[26] and hypertrophic cardiomyopathy (HCM) were characterized in distinct cell configurations: monolayers plated on MEAs and EHTs, respectively. As demonstrated previously, LQT1 phenotype was captured as a prolongation of the QT interval of the field potential[17,26]. As expected, contraction duration measured with MUSCLEMOTION was also prolonged (Figure 5a,b). EHTs were fabricated from an isogenic triplet carrying the $MYH7^{R453C}$ mutation either in homozygosity or heterozygosity and showed a gene dosage effect on the contractility recapitulating disease severity.

Analysis of disease phenotypes *in vivo*

To extend analysis to hearts *in vivo*, we took advantage of the transparency of zebrafish, which allows recording of contracting cardiac tissue *in vivo* (Figure 6a, Supplementary Movie 10). It was previously shown that mutations in G protein β subunit 5 (GNB5) are associated with a multisystem syndrome in human, with severe bradycardia at rest. Zebrafish with loss of function mutations in gnb5a and gnb5b were generated. Consistent with the syndrome manifestation in patients, zebrafish gnb5a/gnb5b double mutant embryos showed severe bradycardia in response to parasympathetic activation[22]. Irregularities in heart rate were visually evident and were clearly

Figure 2: Correlation of results with gold standards.

a) Brightfield image of isolated hPSC-CMs (i), with maximum projection step visually enhanced with a fire Look Up Table (ii), contraction (iii) and velocity (iv) profiles of each individual beat have been generated by MUSCLEMOTION and temporally aligned; linear regression analysis between MUSCLEMOTION results (x-axis) and optical flow results (y-axis) (v). b) Phase contrast image of hPSC-CM monolayers (i), with maximum projection step visually enhanced with a fire Look Up Table (ii), contraction (iii) and velocity (iv) profiles of each individual beat have been generated by MUSCLEMOTION and temporally aligned; linear regression analysis between MUSCLEMOTION results (x-axis) and those obtained with optical flow results (y-axis) (v). c) Phase contrast image of cardiac organoids (i), with maximum projection step visually enhanced with a fire Look Up Table (ii), contraction (iii) and velocity (iv) profiles of each individual beat have been generated by MUSCLEMOTION and temporally aligned; linear regression analysis between MUSCLEMOTION results (x-axis) and those obtained with optical flow results (y-axis) (v). d) Live view of an EHT during contraction analysis. Scale bar = 1 mm. (i), with maximum projection step visually enhanced with a fire Look Up Table (ii), contraction (iii) and velocity (iv) profiles of each individual beat have been generated by MUSCLEMOTION and temporally aligned; linear regression analysis between MUSCLEMOTION results (x-axis) and those obtained with post deflection (y-axis) (v). e) Brightfield image of adult rabbit CMs (i), with maximum projection step visually enhanced with a fire Look Up Table (ii); contraction (iii) and velocity (iv) profiles of each individual beat have been generated by MUSCLEMOTION and temporally aligned; linear regression analysis between MUSCLEMOTION results (x-axis) and those obtained from sarcomere fractional shortening calculation with Fast Fourier Transform (y-axis) (v).

For details on cell sources and cell lines please refer to the Supplementary Table 1.

distinguishable from the wild type counterpart after analysis with MUSCLEMOTION (Figure 6b). Quantification of the heart rate of these zebrafishes with MUSCLEMOTION highly correlated (R^2 = 0.98) with the results of the published manual analyses[22] (Figure 6c). There was however, a striking time-saving for operators in carrying out the analysis using the algorithm (5-10 times faster than manual analysis; 150 recordings were analysed in 5 hours versus 4 days) without compromising accuracy of the outcome. Qualitative analysis of contraction patterns allowed rapid discrimination between arrhythmic vs non-arrhythmic responses to carbachol treatment (Figure 6c).

Finally, we examined human echocardiograms from five healthy and cardiomyopathic individuals (Figure 6d, Supplementary Movie 11). To assess ventricular function, videos were cropped to exclude movement contributions of the atria and valves. MUSCLEMOTION enabled rapid quantification of temporal parameters from standard ultrasound echography (Figure 6e) such as time-to-peak, relaxation time, RR interval and the contraction duration (Figure 6f).

Discussion

A reliable and easy-to-use method to quantify cardiac muscle contraction would be of significant benefit to many basic and clinical science laboratories to characterize cardiac disease phenotypes, understand underlying disease mechanisms and predicting cardiotoxic effects of drugs[15,27]. Quantification of frame-to-frame differences in pixel intensity has been used in recent reports with success[10]; however, the full spectrum of applications for which these algorithms are relevant, how their output data correlates with gold standards in each system and software performance, specifications, license and software availability, have remained unclear.

Here we developed and tested a user-friendly, inexpensive, open source software platform that serves this purpose in a variety of biological systems of heart tissue. Its integration into current research practices would benefit data sharing, reproducibility, comparison and translation in many clinically relevant contexts[28].

The linearity and reliability of MUSCLEMOTION were validated using a 3D reconstructed artificial CM which gave the expected linear correlations between known inputs and the outputs (Figure 1d-f). When random repetitive patterns were applied, amplitude outputs differed from inputs, suggesting a potential limitation to measuring contraction amplitudes in highly repetitive biological samples (such as when sarcomere patterns are well-organized), while temporal parameters remained valid (Figure 1d,e,g). However, conditions such as these would be unlikely in standard biological samples, where camera noise significantly reduces the possibility of saturating pixel movement. We partially attenuated this problem by applying, on user demand, a 10-sigma Gaussian blur filter which significantly increased the accuracy of MUSCLEMOTION with highly repetitive structures. Also, to increase reliability, we built in additional controls to detect any mismatches and errors. MUSCLEMOTION can automatically identify and select the reference frame and increase the signal-to-noise-ratio, features which were particularly relevant in reducing user bias and interaction while improving user experience. MUSCLEMOTION is valid in a wide range of illumination conditions without changing

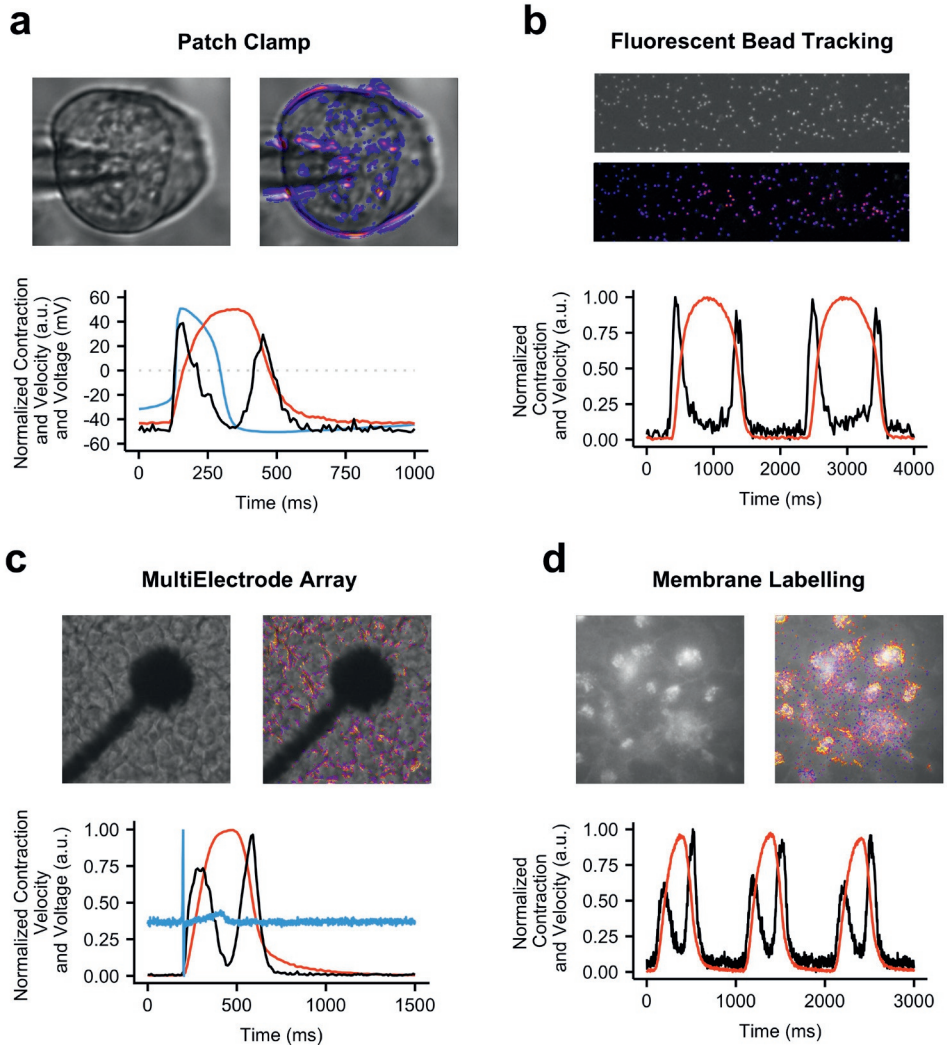

Figure 3: Application of contraction tool to multiple biological situations.

Representative examples with enhancement of moving pixels (top) and profiles (bottom) of contraction (a-d, red), velocity (a-d, black) and voltage (a, c, blue) respectively obtained from high speed movies of patched hPSC-CMs (a), aligned hPSC-CMs on polyacrylamide gels with fluorescent beads (b), monolayers of hiPSC-CMs seeded on MEAs (c) and hPSC-CMs whose membranes have been labelled with CellMask Deep Red (d).

For details on cell sources and cell lines please refer to the Supplementary Table 1.

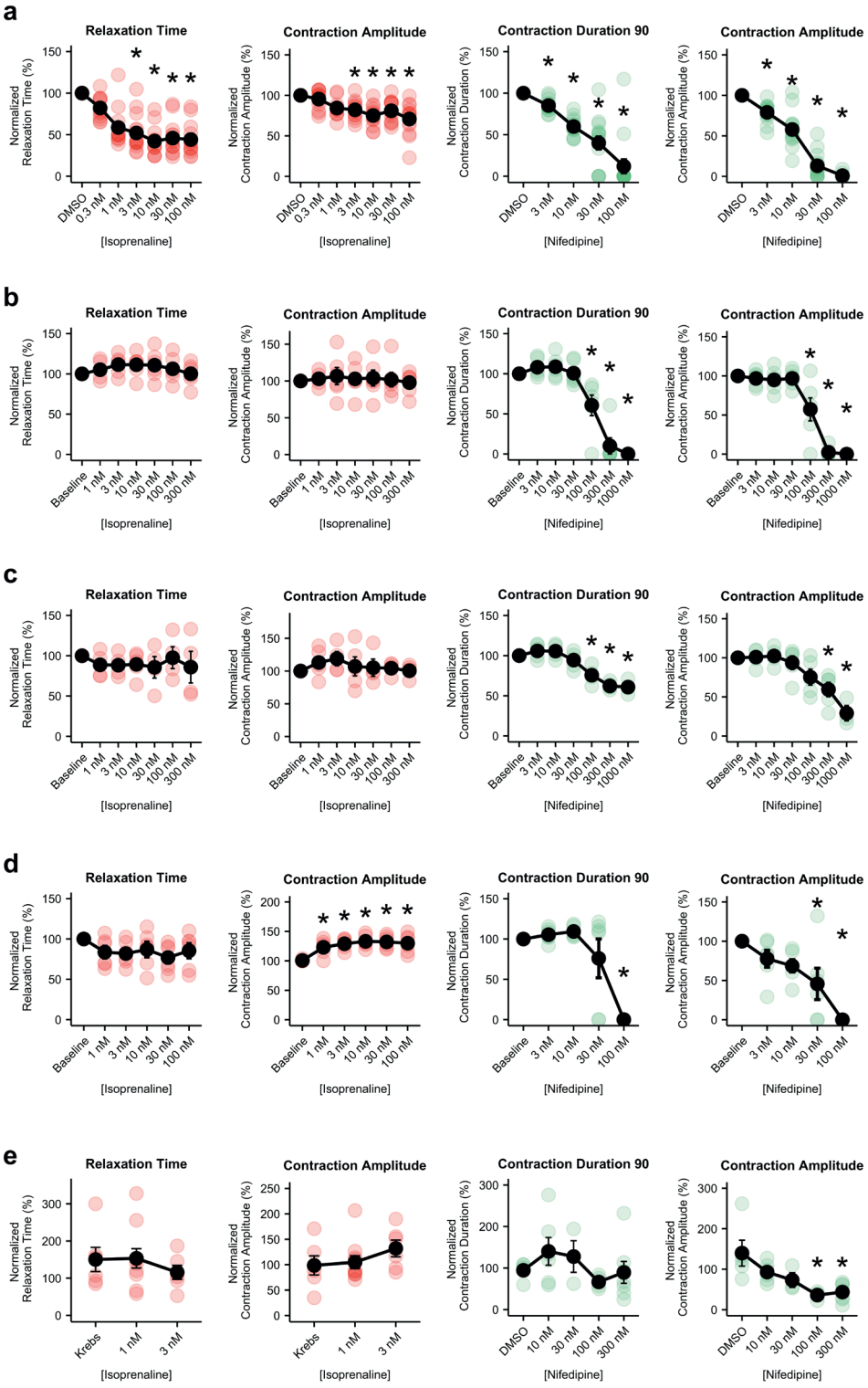
a
Relaxation Time
Normalized Relaxation Time (%)
DMSO 0.3 nM 1 nM 3 nM 10 nM 30 nM 100 nM
[Isoprenaline]
Contraction Amplitude
Normalized Contraction Amplitude (%)
DMSO 0.3 nM 1 nM 3 nM 10 nM 30 nM 100 nM
[Isoprenaline]
Contraction Duration 90
Normalized Contraction Duration (%)
DMSO 3 nM 10 nM 30 nM 100 nM
[Nifedipine]
Contraction Amplitude
Normalized Contraction Amplitude (%)
DMSO 3 nM 10 nM 30 nM 100 nM
[Nifedipine]
b
Relaxation Time
Normalized Relaxation Time (%)
Baseline 1 nM 3 nM 10 nM 30 nM 100 nM 300 nM
[Isoprenaline]
Contraction Amplitude
Normalized Contraction Amplitude (%)
Baseline 1 nM 3 nM 10 nM 30 nM 100 nM 300 nM
[Isoprenaline]
Contraction Duration 90
Normalized Contraction Duration (%)
Baseline 3 nM 10 nM 30 nM 100 nM 300 nM 1000 nM
[Nifedipine]
Contraction Amplitude
Normalized Contraction Amplitude (%)
Baseline 3 nM 10 nM 30 nM 100 nM 300 nM 1000 nM
[Nifedipine]
c
Relaxation Time
Normalized Relaxation Time (%)
Baseline 1 nM 3 nM 10 nM 30 nM 100 nM 300 nM
[Isoprenaline]
Contraction Amplitude
Normalized Contraction Amplitude (%)
Baseline 1 nM 3 nM 10 nM 30 nM 100 nM 300 nM
[Isoprenaline]
Contraction Duration 90
Normalized Contraction Duration (%)
Baseline 3 nM 10 nM 30 nM 100 nM 300 nM 1000 nM
[Nifedipine]
Contraction Amplitude
Normalized Contraction Amplitude (%)
Baseline 3 nM 10 nM 30 nM 100 nM 300 nM 1000 nM
[Nifedipine]
d
Relaxation Time
Normalized Relaxation Time (%)
Baseline 1 nM 3 nM 10 nM 30 nM 100 nM
[Isoprenaline]
Contraction Amplitude
Normalized Contraction Amplitude (%)
Baseline 1 nM 3 nM 10 nM 30 nM 100 nM
[Isoprenaline]
Contraction Duration 90
Normalized Contraction Duration (%)
Baseline 3 nM 10 nM 30 nM 100 nM
[Nifedipine]
Contraction Amplitude
Normalized Contraction Amplitude (%)
Baseline 3 nM 10 nM 30 nM 100 nM
[Nifedipine]
e
Relaxation Time
Normalized Relaxation Time (%)
Krebs 1 nM 3 nM
[Isoprenaline]
Contraction Amplitude
Normalized Contraction Amplitude (%)
Krebs 1 nM 3 nM
[Isoprenaline]
Contraction Duration 90
Normalized Contraction Duration (%)
DMSO 10 nM 30 nM 100 nM 300 nM
[Nifedipine]
Contraction Amplitude
Normalized Contraction Amplitude (%)
DMSO 10 nM 30 nM 100 nM 300 nM
[Nifedipine]

temporal parameters; however, exposure time was linearly correlated with contraction amplitude (Supplementary Figure 7). Furthermore, a series of conditions in which there is no contraction has been used as a negative control (Supplementary Figure 8). Batch mode analyses and data storage in custom folders were also incorporated to support overnight automated analyses. For accurate quantification of amplitude, time-to-peak and relaxation time, an appropriate sampling rate should be chosen. For applications similar to those described here, we recommend recording rates higher than 70 frames per second to sample correctly the fast upstroke of the time-to-peak typical of cardiac tissue. This recording rate is easily achievable even using smartphone slow motion

Figure 4: Pharmacological challenge with positive and negative inotropic compounds.

a) Average dose-response curves (black traces) and single measurements for several parameters obtained in isolated, spontaneously beating, aligned hPSC-CMs treated with isoprenaline (left, red) and nifedipine (right, green). b) Average dose-response curves (black traces) and single measurements for several parameters obtained from monolayers of hPSC-CMs treated with isoprenaline (left, red) and nifedipine (right, green). c) Average dose-response curves (black traces) and single measurements for several parameters obtained in cardiac organoids treated with isoprenaline (left, red) and nifedipine (right, green). d) Average dose-response curves (black traces) and single measurements for several parameters obtained in EHTs treated with isoprenaline (left, red) and nifedipine (right, green). e) Average dose-response curves (black traces) and single measurements for several parameters obtained in adult rabbit CMs treated with isoprenaline (left, red) and verapamil (right, green).

Average data points (black) represent mean ± standard error of mean. For details on cell sources and cell lines please refer to the Supplementary Table 1.

Data information: P-values DMSO versus dose. Panel a i) 0.3 nM: 0.2897; 1 nM: $3.4{\cdot}10^{-6}$; 3 nM: $3.8{\cdot}10^{-8}$; 10 nM: $7{\cdot}10^{-11}$; 30 nM: $7.3{\cdot}10^{-10}$; 100 nM: $2.4{\cdot}10^{-10}$. Panel a ii) 0.3 nM: 1; 1 nM: 0.0645; 3 nM: 0.0136; 10 nM: $8.2{\cdot}10^{-5}$; 30 nM: 0.0063; 100 nM: $2.4{\cdot}10^{-6}$. (N=14; 14; 14; 14; 14; 14; 14) Panel a iii) 3 nM: 0.6533; 10 nM: $4{\cdot}10^{-5}$; 30 nM: $2{\cdot}10^{-9}$; 100 nM: $1.5{\cdot}10^{-15}$. Panel a iv) 3 nM: 0.00054; 10 nM: $1.9{\cdot}10^{-11}$; 30 nM: $< 2{\cdot}10^{-16}$; 100 nM: $< 2{\cdot}10^{-16}$. (N=14; 14; 14; 14; 14) P-values baseline versus dose. Panel b i) 1 nM: 1; 3 nM: 1; 10 nM: 1; 30 nM: 1; 100 nM: 1; 300 nM: 1. Panel b ii) 1 nM: 1; 3 nM: 1; 10 nM: 1; 30 nM: 1; 100 nM: 1; 300 nM: 1. (N=6; 5; 6; 6; 6; 6; 6) Panel b iii) 3 nM: 1; 10 nM: 1; 30 nM: 1; 100 nM: 0.00801; 300 nM: $2.7{\cdot}10^{-9}$; 1000 nM: $1.8{\cdot}10^{-10}$. Panel b iv) 3 nM: 1; 10 nM: 1; 30 nM: 1; 100 nM: 0.00084; 300 nM: $2.9{\cdot}10^{-11}$; 1000 nM: $1.5{\cdot}10^{-11}$. (N=6; 6; 6; 6; 6; 6) P-values baseline versus dose. Panel c i) 1 nM: 1; 3 nM: 1; 10 nM: 1; 30 nM: 1; 100 nM: 1; 300 nM: 1. Panel c ii) 1 nM: 1; 3 nM: 1; 10 nM: 1; 30 nM: 1; 100 nM: 1; 300 nM: 1. (N=5; 5; 4; 5; 4; 4; 4) Panel c iii) 3 nM: 1; 10 nM: 1; 30 nM: 1; 100 nM: 0.00181; 300 nM: $2.9{\cdot}10^{-6}$; 1000 nM: $1.7{\cdot}10^{-5}$. Panel c iv) 3 nM: 1; 10 nM: 1; 30 nM: 1; 100 nM: 0.54836; 300 nM: 0.01392; 1000 nM: $8.2{\cdot}10^{-5}$. (N=5; 5; 4; 5; 5; 5; 3) P-values baseline versus dose. Panel d i) 1 nM: 1; 3 nM: 1; 10 nM: 1; 30 nM: 0.47; 100 nM: 1. Panel d ii) 1 nM: 0.02318; 3 nM: 0.00170; 10 nM: 0.00028; 30 nM: 0.00044; 100 nM: 0.00113. (N=5; 5; 5; 5; 5; 5). Panel d iii) 3 nM: 1; 10 nM: 1; 30 nM: 1; 100 nM: $3{\cdot}10^{-5}$. Panel d iv) 3 nM: 1; 10 nM: 0.49856; 30 nM: 0.01473; 100 nM: $7{\cdot}10^{-6}$. (N=6; 6; 6; 6; 6) P-values Krebs versus dose. Panel e i) 1 nM: 1; 3 nM: 1. Panel e ii) 1 nM: 1; 3 nM: 0.54. (N=6; 10; 7) P-values DMSO versus dose. Panel e iii) 10 nM: 1; 30 nM: 1; 100 nM: 1; 300 nM: 1. Panel e iv) 10 nM: 0.5298; 30 nM: 0.2470; 100 nM: 0.0054; 300 nM: 0.0029. (N=7; 8; 4; 5; 7).

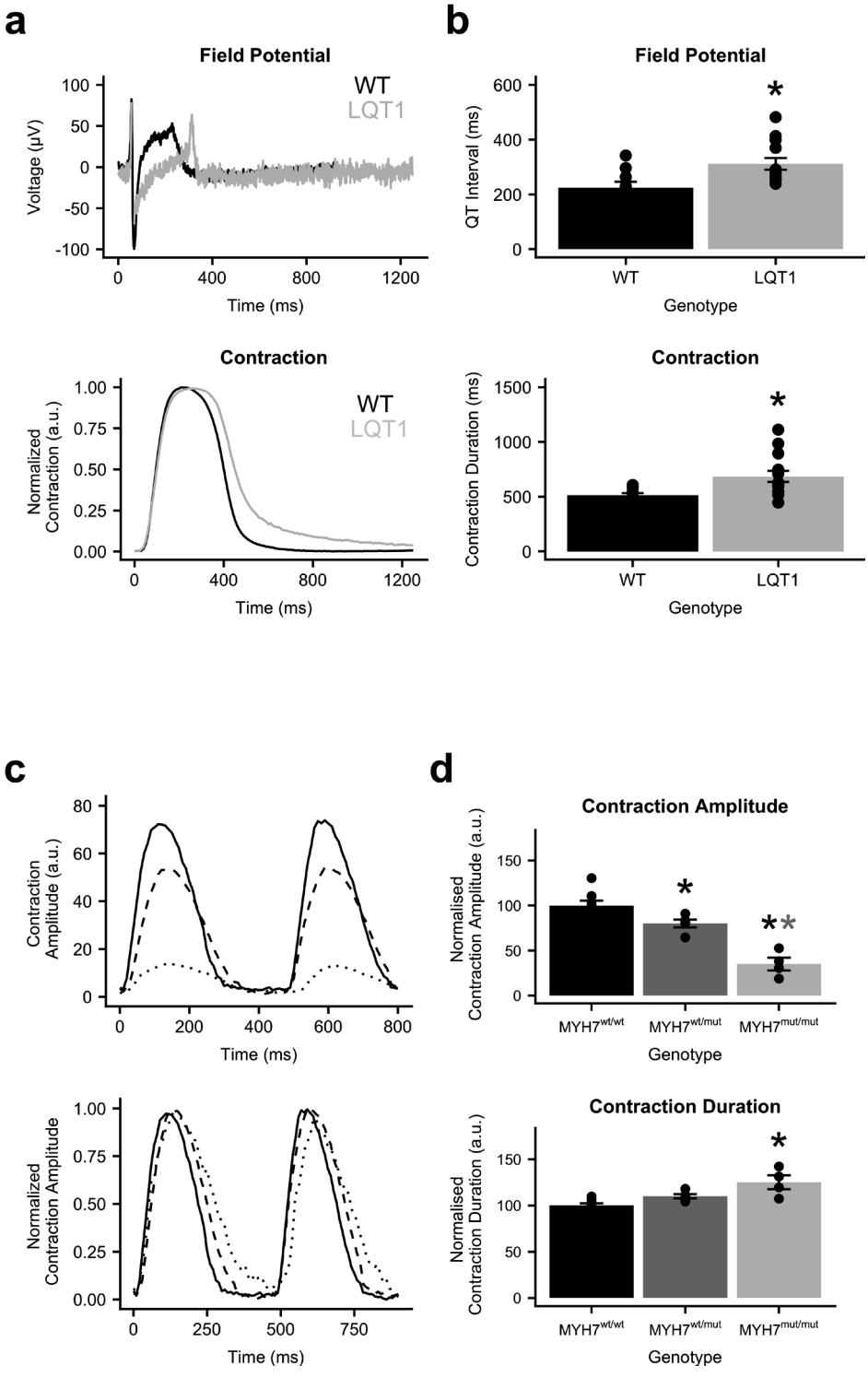
a
Field Potential
WT
LQT1
Voltage (μV)
100
50
0
-50
-100
0
400
800
1200
Time (ms)
b
Field Potential
QT Interval (ms)
600
400
200
0
*
WT
LQT1
Genotype
Contraction
Normalized Contraction (a.u.)
1.00
0.75
0.50
0.25
0.00
WT
LQT1
Time (ms)
Contraction
Contraction Duration (ms)
1500
1000
500
0
*
WT
LQT1
Genotype
c
Contraction Amplitude (a.u.)
80
60
40
20
0
0
200
400
600
800
Time (ms)
Normalized Contraction Amplitude
1.00
0.75
0.50
0.25
0.00
0
250
500
750
Time (ms)
d
Contraction Amplitude
Normalised Contraction Amplitude (a.u.)
150
100
50
0
*
**
MYH7wt/wt
MYH7wt/mut
MYH7mut/mut
Genotype
Contraction Duration
Normalised Contraction Duration (a.u.)
150
100
50
0
*
MYH7wt/wt
MYH7wt/mut
MYH7mut/mut
Genotype

video options (~120/240 frames per second), obviating the need for dedicated cameras and recording equipment if necessary.

We demonstrated excellent linear correlations between our software tool and multiple other standard methods independent of substrate, cell configuration and technology platform and showed that MUSCLEMOTION is able to capture contraction in a wide range of *in vivo* and *in vitro* applications (Figure 2 and Figure 3). Specifically, we identified several advantages compared to optical flow algorithms in terms of speed and the absence of arbitrary binning factors or thresholds which, when modified, profoundly affect the results. One limitation compared to optical flow or EHT standard algorithm is that the tool lacks qualitative vector orientation, making it more difficult to assess contraction direction. Particularly important was the correlation with force data calculated from the displacement of flexible posts by EHTs. This indicates that when the mechanical properties of substrates are known[29], MUSCLEMOTION allows absolute quantification of contractile force. Technical limitations of the EHT recording system allowed us to analyze only movies with JPEG compression; this resulted in loss of pixel information that might have negatively influenced the correlation shown. For better and more accurate results on contraction quantification, non-lossy/uncompressed video formats should be used for recordings since individual pixel information is lost upon compression and therefore not available for analysis by MUSCLEMOTION.

We proposed and validated practical application in pharmacological challenges using multiple biological preparations recorded in different laboratories; this means that immediate use in multiple independent high-throughput drug-screening pipelines is possible without further software development being required, as recently applied for a drug screening protocol on cardiac organoids from hPSCs[18]. Intuitively, the possibility of having inter-assay comparisons will also be of particular relevance where comparisons of contraction data across multiple platforms are required by regulatory agencies or consortia (e.g. CiPA, CSAHi)[5,6,25,30]. Moreover, this might offer a quantitative approach

Figure 5: *In vitro* disease phenotypes.

a) Field potential and contraction profile of wildtype (black) and LQT1 (gray) hPSC-CM monolayers on MEAs. b) Quantitative analysis of the QT interval and the contraction duration. c) Raw (top) and normalized (bottom) contraction profiles of HCM-EHTs from $MYH7^{wt/wt}$ (solid), $MYH7^{wt/mut}$ (dashed), $MYH7^{mut/mut}$ (dotted) cell lines. d) Quantitative analysis of contraction amplitude and contraction duration.

Data information: P-values QT-interval: WT versus LQT1: 0.012. P-values contraction duration: WT versus LQT1: 0.012. P-values contraction amplitude: $MYH7^{wt/wt}$ versus $MYH7^{wt/mut}$: 0.026; $MYH7^{wt/wt}$ versus $MYH7^{mut/mut}$: $6{\cdot}10^{-6}$; $MYH7^{wt/mut}$ versus $MYH7^{mut/mut}$: 0.00065. P-values contraction duration: $MYH7^{wt/wt}$ versus $MYH7^{wt/mut}$: 0.062; $MYH7^{wt/wt}$ versus $MYH7^{mut/mut}$: 0.00085; $MYH7^{wt/mut}$ versus $MYH7^{mut/mut}$: 0.0046.

to investigating how genetic or acquired diseases of the heart (e.g. cardiomyopathies[7], Long QT Syndrome[31]), heart failure resulting from anticancer treatments[32,33] or maturation strategies[20,34,35] affect cardiac contraction. The possibility of linking *in vitro* with *in vivo* assays, with low cost technologies applicable with existing hardware certainly represents an advantage as demonstrated by automatic quantification of zebrafish heartbeats and human echocardiograms (Figure 6). Overall, these results clearly demonstrated that contraction profiles could be derived and quantified in a wide variety of commonly used experimental and clinical settings. MUSCLEMOTION might represent a starting point for a swift screening method to provide clinically relevant insights into regions of limited contractility in the hearts of patients. We encourage further development of this open source platform to fit specific needs; future areas of application could include skeletal or smooth muscle in the same range of formats described here.

MUSCLEMOTION allows the use of a single, transparent method of analysis of cardiac contraction in many modalities for rapid and reliable identification of disease phenotypes, potential cardiotoxic effects in drug screening pipelines and translational comparison of contractile behaviour.

Limitations

Saturation of pixel movements may affect contraction amplitudes. However, as demonstrated with the artificial CM, contraction velocity and all temporal parameters remained valid. We also minimized the impact of highly repetitive structures on the

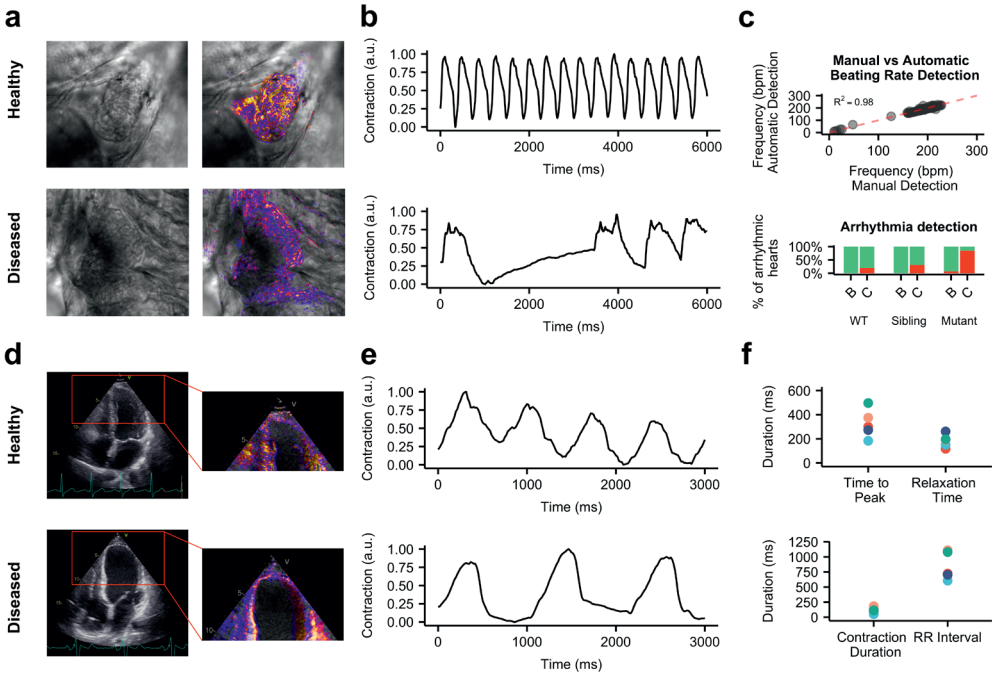

output of MUSCLEMOTION by applying a Gaussian filter, which also helped in reducing the impact of transverse movements on contraction profiles. High frequency contraction might complicate baseline detection, especially if the duration of the contracted state is similar to that of the relaxed (e.g. approaching sinusoidal). We have implemented a "fast mode" option that captures reliable baseline values even at high contraction rates. MUSCLEMOTION does not measure absolute values of cell shortening or force of contraction. However, as demonstrated by correlations with these physical quantities (Figure 2d,e v), specific setups can be calibrated to obtain such readout.

Adult CMs contract dominantly along the longitudinal axis. However, hPSC-CMs are highly variable in shape, often showing concentric contractions, so that effects of transverse movement are usually intrinsic to the experimental model and they should be considered in the global contraction analysis. Indirect transverse movements originating from uncontrolled experimental conditions or moving objects other than those of interest (e.g. vibrations, sample shift, floating debris, air bubbles) should be avoided since they might lead to overestimation of the cardiomyocyte contraction.

Methods

Extended methods are in the Supplementary Information. The datasets generated and/or analyzed during the current study are available from the corresponding authors on reasonable request.

Figure 6: *In vivo* disease phenotypes.

a) Representative examples of wild type (top) and gnb5a/gnb5b mutant (bottom) zebrafishes and relative enhancement of moving pixels. b) Representative qualitative analyses of normal (top) and arrhythmic (bottom) contraction profiles from wild type and gnb5a/gnb5b mutant zebrafishes treated with carbachol. c) Correlation of results obtained from manual (x-axis) vs automatic (y-axis) detection of beating frequency (top); distribution of normal (green) and arrhythmic (red) contraction patterns in baseline condition (B) and after treatment with carbachol (C) in wild type and gnb5a/gnb5b mutant zebrafishes (bottom). d) Representative echocardiograms of healthy (top) and cardiomyopathic (bottom) human individuals. Ventricles have been manually cropped and the enhancement of moving pixels is overlaid. e) Representative qualitative analyses of normal (top) and poor (bottom) ventricular functions. f) Quantitative data collected from echocardiogram in 5 individuals. Each colour represents one individual.

Code Availability
MUSCLEMOTION source code has been written in the ImageJ Macro Language and is available for use and further development.

Model Cell
The *in silico* cardiomyocyte-like model (Figure 1d,f,g) was created using Blender v2.77.

Optical Flow analysis
Optical flow analysis was implemented in LabVIEW as described by Hayakawa et al.[12,13].

Generation of hiPSC-HCM isogenic triplet using CRISPR/Cas9
Dual guide RNA/Cas9-Nickase strategy was designed to introduce the MYH7-C9123T SNP (encoding the R453C-β-MHC modification) in ReBL-PAT hiPSC line, as previously described[14].

hPSC Culture and Differentiation
hPSCs from multiple independent cell lines (Supplementary Table 1) were differentiated to CMs as previously described[15-18], or with the Pluricyte® Cardiomyocyte Differentiation Kit (Pluriomics b.v.) according to the manufacturer's protocol. Experiments were performed at 18-30 days after initiation of differentiation, depending on the cell source and configuration. Pluricytes® were kindly provided by Pluriomics b.v.

Patch Clamp Recordings on hPSC-CMs
Electrophysiological recordings of isolated hPSC-CMs were performed as previously described[17].

MEA Recordings of hPSC-CMs
Field potentials from MEAs were recorded and analyzed as previously published[19].

Movement of embedded beads
Gelatin-patterned polyacrylamide gels containing fluorescent beads were generated and analyzed as described previously[20].

Monolayers of hPSC-CMs
25k-40k cells were plated per Matrigel-coated glass ø10 mm coverslip.

Cardiac Organoids
Cardiac organoids composed of hPSC-CMs and hPSC-derived endothelial cells, were generated as previously described[18].

Adult cardiomyocytes
CMs were isolated from New Zealand White male rabbits as previously described[21].

Membrane labelling
hPSC-CMs were plated on Matrigel-coated glass-bottom 24-well plates and labelled with CellMask Deep Red according to the manufacturer's instructions.

Engineered heart tissues
EHTs were generated and analyzed as previously described[15].

Zebrafish hearts
Zebrafish hearts were recorded, treated and analysed as previously described[22].

Echocardiograms
Anonymized ultrasounds of 5 adult patients were selected from the echocardiography database of the Leiden University Medical Center.

Statistics
One-way ANOVA for paired or unpaired measurements was applied to test the differences in means on normalized drug effects. P-values obtained from two-tailed pairwise comparisons were corrected for multiple testing using Bonferroni's method. Statistical analyses were performed with R v3.3.3. P-values lower than 0.05 were considered statistically significant and indicated with an asterisk (*). N-values represent biological repeats.

Sources of Funding
This work was initiated in the context of the National Centre for the Replacement, Refinement, and Reduction of Animals in Research CRACK IT InPulse project code 35911 to 259146, with support from GlaxoSmithKline. It was supported by the following grants: ERC-AdG (European Research Council - Advanced Grant) STEMCARDIOVASC (C.L. Mummery, B.J. van Meer, E. Giacomelli, M. Bellin, and L.G.J. Tertoolen), ZonMW (ZorgOnderzoek Nederland - Medische wetenschappen) MKMD (Meer Kennis met Minder Dieren) Applications of Innovations 2015 to 2016 (C.L. Mummery, M. Bellin, and L. Sala), BHF (British Heart Foundation) grants SP/15/9/31605 and PG/14/59/31000 and BIRAX 04BX14CDLG grants (C. Denning), ERC-AdG IndivuHeart (T. Eschenhagen), DZHK (German Centre for Cardiovascular Research; T. Eschenhagen, U. Saleem, A. Hansen, and I. Mannhardt), ERC-StG (European Research Council - Starting Grant) StemCardioRisk (R.P. Davis and M.P.H. Mol), and the Netherlands Organisation for Scientific Research grant VIDI-917.15.303 (R.P. Davis and C. Grandela). The Dutch Heart Foundation: CVON (Cardiovasculair Onderzoek Nederland) 2012–10 Predict project (C.D. Koopman), E-Rare–CoHeart project (S.M. Kamel), and CVON–HUSTCARE 2013 to 2018 (C.L. Mummery and L. Sala).

References

1. Laverty, H. G. *et al*. How can we improve our understanding of cardiovascular safety liabilities to develop safer medicines? *Br J Pharmacol*. **163,** 675–693 (2011).

2. Passier, R., Orlova, V. V. & Mummery, C. L. Complex Tissue and Disease Modeling using hiPSCs. *Cell Stem Cell*. **18,** 309–321 (2016).

3. Bellin, M., Marchetto, M. C., Gage, F. H. & Mummery, C. L. Induced pluripotent stem cells: the new patient? *Nat Rev Mol Cell Biol*. **13,** 713–726 (2012).

4. van Meer, B. J., Tertoolen, L. G. J. & Mummery, C. L. Concise Review: Measuring Physiological Responses of Human Pluripotent Stem Cell Derived Cardiomyocytes to Drugs and Disease. *Stem Cells*. **34,** 2008–2015 (2016).

5. Kitaguchi, T. *et al*. CSAHi study: Evaluation of multi-electrode array in combination with human iPS cell-derived cardiomyocytes to predict drug-induced QT prolongation and arrhythmia - Effects of 7 reference compounds at 10 facilities. *J Pharmacol Toxicol Methods*. **78,** 93–102 (2016).

6. Hwang, H. S. *et al.* Comparable calcium handling of human iPSC-derived cardiomyocytes generated by multiple laboratories. *J Mol Cell Cardiol*. **85,** 79–88 (2015).

7. Birket, M. J. *et al.* Contractile Defect Caused by Mutation in MYBPC3 Revealed under Conditions Optimized for Human PSC-Cardiomyocyte Function. *Cell Rep*. **13,** 733–745 (2015).

8. Ribeiro, A. J. S. *et al.* Contractility of single cardiomyocytes differentiated from pluripotent stem cells depends on physiological shape and substrate stiffness. *Proc Natl Acad Sci USA*. **112,** 12705–12710 (2015).

9. Ribeiro, A. J. S. *et al.* Multi-Imaging Method to Assay the Contractile Mechanical Output of Micropatterned Human iPSC-Derived Cardiac Myocytes. *Circ Res*. **120,** 1572–1583 (2017).

10. Kijlstra, J. D. *et al.* Integrated Analysis of Contractile Kinetics, Force Generation, and Electrical Activity in Single Human Stem Cell-Derived Cardiomyocytes. *Stem Cell Reports*. **5,** 1226–1238 (2015).

11. Stoehr, A. *et al.* Automated analysis of contractile force and Ca2+ transients in engineered heart tissue. *Am J Physiol Heart Circ Physiol*. **306,** H1353–63 (2014).

12. Hayakawa, T. *et al.* Image-based evaluation of contraction–relaxation kinetics of human-induced pluripotent stem cell-derived cardiomyocytes: Correlation and complementarity with extracellular electrophysiology. *J Mol Cell Cardiol*. **77,** 178–191 (2014).

13. Hayakawa, T. *et al.* Noninvasive evaluation of contractile behavior of cardiomyocyte monolayers based on motion vector analysis. *Tissue Eng Part C Methods*. **18,** 21–32 (2012).

14. Ran, F. A. *et al.* Genome engineering using the CRISPR-Cas9 system. *Nat Protoc*. **8,** 2281–2308 (2013).

15. Mannhardt, I. *et al.* Human Engineered Heart Tissue: Analysis of Contractile Force. *Stem Cell Reports*. **7,** 29–42 (2016).

16. van den Berg, C. W., Elliott, D. A., Braam, S. R., Mummery, C. L. & Davis, R. P. Differentiation of Human Pluripotent Stem Cells to Cardiomyocytes Under Defined Conditions. *Methods Mol Biol*. **1353,** 163–180 (2016).

17. Sala, L. *et al.* A new hERG allosteric modulator rescues genetic and drug-

induced long-QT syndrome phenotypes in cardiomyocytes from isogenic pairs of patient induced pluripotent stem cells. *EMBO Mol Med*. **8,** 1065–1081 (2016).

18. Giacomelli, E. *et al.* Three-dimensional cardiac microtissues composed of cardiomyocytes and endothelial cells co-differentiated from human pluripotent stem cells. *Development* **144,** dev.143438–1017 (2017).

19. Sala, L., Ward-van Oostwaard, D., Tertoolen, L. G. J., Mummery, C. L. & Bellin, M. Electrophysiological Analysis of human Pluripotent Stem Cell-derived Cardiomyocytes (hPSC-CMs) Using Multi-electrode Arrays (MEAs). *J Vis Exp*. (2017)

20. Ribeiro, M. C. *et al.* Functional maturation of human pluripotent stem cell derived cardiomyocytes *in vitro*-correlation between contraction force and electrophysiology. *Biomaterials*. **51,** 138–150 (2015).

21. MacQuaide, N., Ramay, H. R., Sobie, E. A. & Smith, G. L. Differential sensitivity of Ca^{2+} wave and Ca^{2+} spark events to ruthenium red in isolated permeabilised rabbit cardiomyocytes. *J Physiol (Lond)*. **588,** 4731–4742 (2010).

22. Lodder, E. M. *et al.* GNB5 Mutations Cause an Autosomal-Recessive Multisystem Syndrome with Sinus Bradycardia and Cognitive Disability. *Am J Hum Genet*. **99,** 704–710 (2016).

23. Rocchetti, M. *et al.* Ranolazine prevents INaL enhancement and blunts myocardial remodelling in a model of pulmonary hypertension. *Cardiovasc Res*. **104,** 37–48 (2014).

24. Bers, D. M. Cardiac excitation-contraction coupling. *Nature* **415,** 198–205 (2002).

25. Sala, L., Bellin, M. & Mummery, C. L. Integrating cardiomyocytes from human pluripotent stem cells in safety pharmacology: has the time come? *Br J Pharmacol*. **97,** 2684 (2016).

26. Zhang, M. *et al.* Recessive cardiac phenotypes in induced pluripotent stem cell models of Jervell and Lange-Nielsen syndrome: disease mechanisms and pharmacological rescue. *Proc Natl Acad Sci USA*. **111,** E5383–92, (2014).

27. Rodriguez, M. L. *et al.* Measuring the contractile forces of human induced pluripotent stem cell-derived cardiomyocytes with arrays of microposts. *J Biomech Eng*. **136,** 051005 (2014).

28. Bullen, A. Microscopic imaging techniques for drug discovery. *Nat Rev Drug Discov*. **7,** 54–67 (2008).

29. Vandenburgh, H. *et al.* Drug-screening platform based on the contractility of tissue-engineered muscle. *Muscle Nerve*. **37,** 438–447 (2008).

30. Cavero, I. & Holzgrefe, H. Comprehensive *in vitro* Proarrhythmia Assay, a novel *in vitro*/*in silico* paradigm to detect ventricular proarrhythmic liability: a visionary 21st century initiative. *Expert Opin Drug Saf*. **13,** 745–758 (2014).

31. Rocchetti, M. *et al.* Elucidating arrhythmogenic mechanisms of long-QT syndrome CALM1-F142L mutation in patient-specific induced pluripotent stem cell-derived cardiomyocytes. *Cardiovasc Res*. **113,** 531–541 (2017).

32. Burridge, P. W. *et al.* Human induced pluripotent stem cell-derived cardiomyocytes recapitulate the predilection of breast cancer patients to doxorubicin-induced cardiotoxicity. *Nat Med*. **22,** 547–556 (2016).

33. Bellin, M. & Mummery, C.L. Stem

cells: The cancer's gone, but did chemotherapy damage your heart? *Nat Rev Cardiol*. **13,** 383–384 (2016).

34. Nunes, S. S. *et al.* Biowire: a platform for maturation of human pluripotent stem cell-derived cardiomyocytes. *Nat Meth*. **10,** 781–787 (2013).

35. Chan, Y-C. *et al.* Electrical stimulation promotes maturation of cardiomyocytes derived from human embryonic stem cells. *J Cardiovasc Transl Res*. **6,** 989–999 (2013).

Supplementary information

Supplementary Methods

Model cell

To establish and test the algorithm of MUSCLEMOTION we first created an *in silico* CM-like shape (Figure 1d,f,g) using Blender v2.77 (Stichting Blender Foundation). This three-dimensional squared sphere had an aspect ratio of 1:1:0.26 (XYZ) when contracted and 2:1:0.26 (XYZ) when relaxed. A diffuse "shader" with a foggy, patterned texture was then applied to the object to simulate extremely repetitive phase contrast image features. Temporal input parameters were then imposed: 100 ms for time-to-peak (t_1) and 350 ms for relaxation time (t_2). A beating frequency of 1 Hz and sampling rate of 100 frames per second were simulated. Modifications of cell shortening (25% and 50% of baseline) and time-to-peak (50% and 200% of baseline) were generated to validate the algorithm linearity.

Patch clamp recordings on hPSC-CMs

Electrophysiological recordings of isolated hPSC-CMs were performed using the perforated patch clamp technique as previously described[1]. Briefly, cells were paced at 1 Hz through the glass capillary and were perfused with warm (37 °C) Tyrode's solution containing (mM): 154 NaCl, 5.4 KCl, 1.8 $CaCl_2$, 1 $MgCl_2$, 5 HEPES-NaOH, 5.5 D-Glucose; pH was adjusted to 7.35 with NaOH. Pipette solution contained (mM): 125 K-Gluconate, 20 KCl, 10 NaCl, 10 HEPES; pH was adjusted to 7.2 with KOH. Amphotericin-B was dissolved in DMSO right before each experiment and added to the pipette solution to reach a final concentration of 0.22 mM.

Movement of embedded beads

Fabrication of gelatin-patterned polyacrylamide gels containing fluorescent beads and contraction force measurements were performed as described previously2, with an increased recording frame rate to 56 frames per second. For nifedipine experiments, cells were paced through an external stimulator to ensure a constant and triggered beating rate. Experiments with isoprenaline were performed in spontaneously beating aligned hPSC-CMs to investigated the pharmacological effect on beat rate. hPSC-CMs on patterned polyacrylamide gels were measured in Pluricyte® medium (Pluriomics b.v.). Drug treatment was performed with additive doses which were compared to baseline.

Monolayers of hPSC-CMs

Pluricytes® (Pluriomics b.v.) were cultured following the manufacturer's instructions. Cells were plated at a density of 25k-40k cells/coverslip on Matrigel-coated glass ø10 mm coverslips for 7 days before measurements of contraction. Monolayers were paced by an external field stimulator (bipolar square pulse of ~15 V for 5 ms) and superfused with a warm (37 °C) Tyrode's solution (described above). Drug treatment was performed with additive doses which were compared to baseline.

Cardiac organoids

Cardiac organoids composed of hPSC-CMs and hPSC-derived endothelial cells were generated as previously described[3]. Cardiac organoids were paced through an external field stimulator (bipolar square pulse of ~15 V for 5 ms) and superfused with a warm

(37 °C) Tyrode's solution (described above). Drug treatment was performed with additive doses which were normalized to baseline.

Adult cardiomyocytes

CMs were isolated from New Zealand White male rabbits as previously described[4]. Animal experiments complied with the ARRIVE guideline for animal studies. The procedures used complied with current regulations and were approved by the Research Committee of the University of Glasgow. In total, 3 animals were used for these experiments. Sarcomere shortening was estimated using an ImageJ macro that calculates, for each image in a stack, the spatial frequency of the pixel intensity profile along a fixed, elongated rectangular region of interest placed inside the cell boundary and on a part of the cell showing clear banding. At each time point, mean sarcomere length corresponded to the location of the peak frequency value of the power spectrum obtained by taking the Fourier Transform of the intensity profile. Drug treatment was performed with single dose additions which were normalized to their pre-treatment baseline.

Membrane labelling

hPSC-CMs were plated on Matrigel-coated glass-bottom 24-well plates in either BPEL[5] or Differentiation Medium C (Pluriomics b.v.) at a density between 20k-70k cells per well. Live cells were labelled with Cell Mask Deep Red (Thermo Fisher Scientific Inc.) and imaged with on a Nikon Ti-U Eclipse with a CamRecord CR600x2 monochromatic camera (Optronis GmbH) at 333 Hz after amplification of the image with an intensifier tube (Photonis b.v.).

Engineered heart tissues

EHTs were generated and analyzed as previously described[6]. In brief, hiPSC were differentiated into CMs with a growth factor based protocol in suspension culture using spinner flasks. Following dissociation with collagenase, fibrin-based EHTs were generated with $1x10^6$ cells per 100 µL EHT construct[7]. Contraction analysis based on a video-optical figure recognition algorithm (100 frames per second) was performed under electrical stimulation in serum-free Tyrode's solution in a humidified gas (40% O_2, 7% CO_2) and temperature (37 °C) controlled incubation chamber[8]. Drug treatment was performed with additive doses which were compared to baseline.

Zebrafish hearts

All experiments were conducted in accordance to the ARRIVE guidelines and approved by the local ethics committee of the Koninklijke Nederlandse Akademie van Wetenschappen (KNAW). Wild-type, sibling and *gnb5a/gnb5b* double mutant embryos (5 days post fertilization) were embedded in 0.3% agarose (Ultra Pure agarose, Invitrogen) prepared in E3 medium containing 16 mg/ml tricaine and mounted on glass bottom dishes. Recordings were performed at 28 °C using an inverted light microscope with climate chamber. Recordings were performed at 150 frames per second for 10-30 seconds using a C9300-221 high-speed CCD camera (Hamamatsu Photonics K.K). Basal heart rates were recorded first. Subsequently 400 µM carbachol (CCh; Sigma-Aldrich) was added and incubated for 30 min before heart rates were measured a second time.

Echocardiograms
Anonymized ultrasounds of 5 adult patients who had undergone transthoracic echocardiography between 2012 and 2017 on clinical indication, were selected from the echocardiography database of the Leiden University Medical Center. Transthoracic echocardiography was performed using a GE Vivid7 or E9 (GE-Vingmed, Horten, Norway) ultrasound machine with standard views from the parasternal, subcostal, suprasternal and apical window. For MUSCLEMOTION analysis, 4 chamber views were used. The images were converted to avi-format, preferably containing multiple beats. For this analysis of clinically acquired data, the Institutional Review Board waived the need for patient written informed consent.

Supplementary references

1. Sala, L. et al. A new hERG allosteric modulator rescues genetic and drug-induced long-QT syndrome phenotypes in cardiomyocytes from isogenic pairs of patient induced pluripotent stem cells. *EMBO Mol Med.* **8,** 1065–1081 (2016).

2. Ribeiro, M.C. et al. Functional maturation of human pluripotent stem cell derived cardiomyocytes *in vitro*--correlation between contraction force and electrophysiology. *Biomaterials* **51,** 138–150 (2015).

3. Giacomelli, E. et al. Three-dimensional cardiac microtissues composed of cardiomyocytes and endothelial cells co-differentiated from human pluripotent stem cells. *Development* **144,** dev.143438–1017 (2017).

4. MacQuaide, N., Ramay, H.R., Sobie, E.A., Smith, G.L.. Differential sensitivity of Ca^{2+} wave and Ca^{2+} spark events to ruthenium red in isolated permeabilised rabbit cardiomyocytes. *J. Physiol. (Lond)* **588,** 4731–4742 (2010).

5. van den Berg CW, Elliott DA, Braam SR, Mummery CL, Davis RP. Differentiation of Human Pluripotent Stem Cells to Cardiomyocytes Under Defined Conditions. *Methods. Mol. Biol.* **1353,** 163–180 (2016).

6. Mannhardt I, Breckwoldt K, Letuffe-Brenière D, et al. Human Engineered Heart Tissue: Analysis of Contractile Force. *Stem Cell Reports* **7,** 29–42 (2016).

7. Mannhardt I, Saleem U, Benzin A, Schulze T, Klampe B, Eschenhagen T, Hansen A. Automated Contraction Analysis of Human Engineered Heart Tissue for Cardiac Drug Safety Screening. *J Vis Exp.* **122,** 55461 (2017).

8. Hansen A, Eder A, Bonstrup M, Flato M, Mewe M, Schaaf S, Aksehirlioglu B, Schworer A, Uebeler J, Eschenhagen T. Development of a Drug Screening Platform Based on Engineered Heart Tissue. *Circ Res*. **107,** 35–44 (2010).

Supplementary movie legends

Supplementary Movies are available at:
https://doi.org/10.1161/CIRCRESAHA.117.312067

Supplementary Movie 1: test bench of block displacements.

Supplementary Movie 2: single human stem cell derived cardiomyocyte during a patch clamp experiment.

Supplementary Movie 3: human stem cell derived cardiomyocyte monolayer culture.

Supplementary Movie 4: human stem cell derived cardiac organoid.

Supplementary Movie 5: Engineered heart tissue from human stem cell derived cardiomyocytes.

Supplementary Movie 6: isolated adult rabbit cardiomyocyte.

Supplementary Movie 7: Fluorescent bead displacement by a single hPSC-CM aligned on a gelatin patterned polyacrylamide substrate.

Supplementary Movie 8: hPSC-CMs monolayer culture plated on a Multi Electrode Array.

Supplementary Movie 9: Fluorescently labelled hPSC-CMs monolayer.

Supplementary Movie 10: Optical recording of a zebrafish heart (wildtype) *in vivo*.

Supplementary Movie 11: Human echocardiogram from healthy individual.

Supplementary Figures

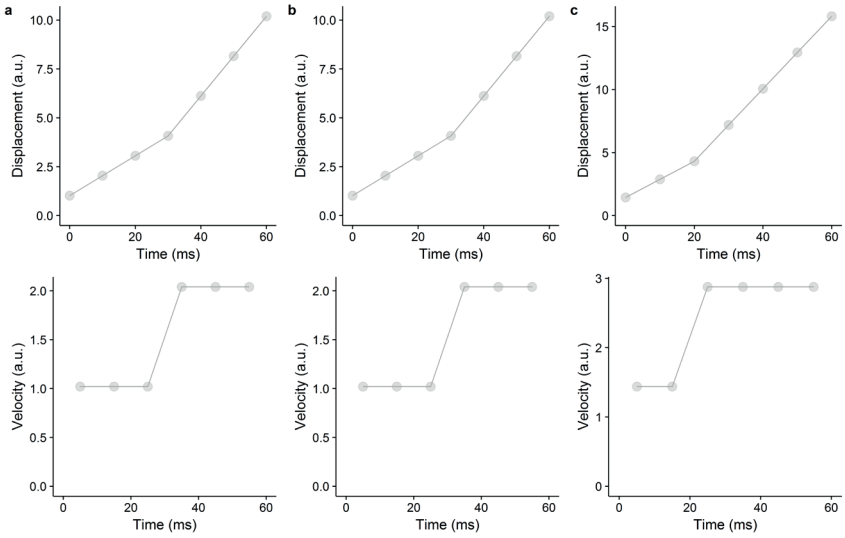

Supplementary Figure 1: Linearity of the contraction tool.

a) Profiles of displacement (top) and velocity (bottom) when the block is moving along the x-axis; b) Profiles of displacement (top) and velocity (bottom) when the block is moving along the y-axis; c) Profiles of displacement (top) and velocity (bottom) when the block is moving along both axes. In all figures, the linearity between displacement and velocity is clearly preserved.

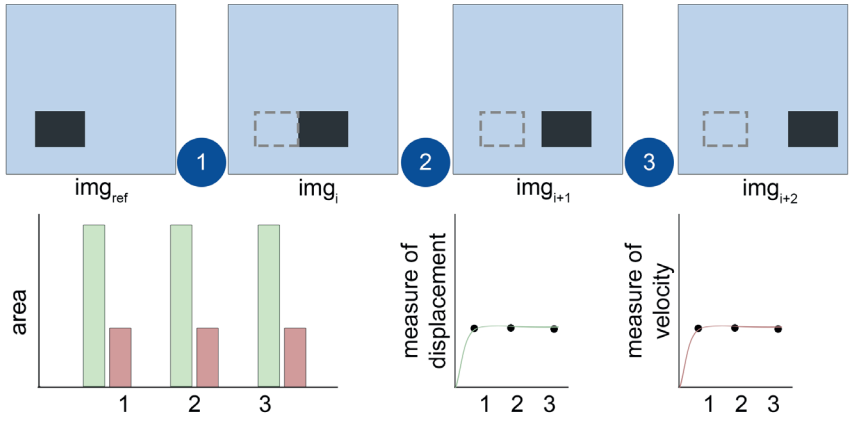

Supplementary Figure 2: Out-of-bounds limitation of the contraction tool.

Demonstration of the out-of-bounds limitation occurring when the differences of moving areas in img_i an img_{i-1} relative to img_{ref} reached the maximum level. This is clearly visible in the clipping of the contraction plot. However, the velocity plot is still valid, since it calculates the difference between img_i and img_{i-1}.

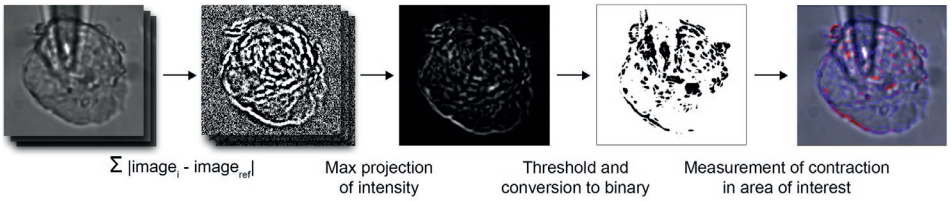

Supplementary Figure 3: Automatic region of interest selection using maximum projection.

First the difference from img_i to img_{ref} is calculated. Next, the projection of the maximum intensity of the resulting image stack is generated. This projection is subjected to a threshold (standard set to the mean intensity of the projection image plus one standard deviation) and made binary. Next, this mask is used to analyze only the moving (contracting) areas.

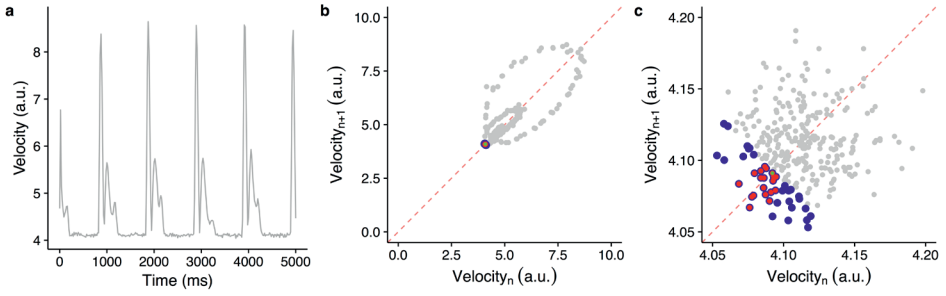

Supplementary Figure 4: Automatic reference frame detection.

a) Example of measured velocity profile; b) Velocity$_n$ values are plotted against velocity$_{n+1}$ values. In order to select the point that has both low velocity and neighbour with similar values (two characteristics of a flat diastolic period, where the derivative is ideally zero) a number of points (in this example 50, blue) are selected that have the smallest distance to the origin; c) Magnification of a region in b). For each of the selected points, a number of points (in this example 20, red) that are closet to the unity line (dotted red) is selected. Finally, of those points, one point (green) is selected as the smallest combination of values and distance from unity line.

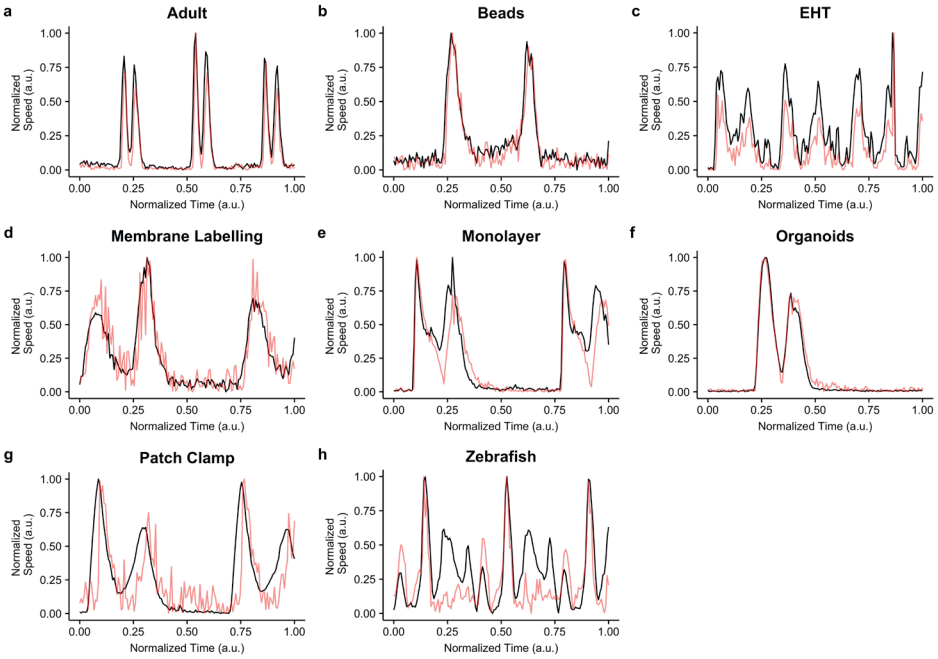

Supplementary Figure 5: Examples of linearity checks for various cardiac models.

The measured speed by frame-to-frame analysis (black) and calculated speed from the frame to reference frame analysis (red) of a) isolated adult rabbit cardiomyocyte contraction; b) fluorescent bead displacement by hPSC-CM on gelatin patterned polyacrylamide; c) engineered heart tissue contraction; d) contraction of fluorescently labelled monolayer; e) hPSC-CM monolayer contraction; f) hPSC-CM organoid contraction; g) single hPSC-CM contraction during patch clamp; h) zebrafish heart *in vivo*.

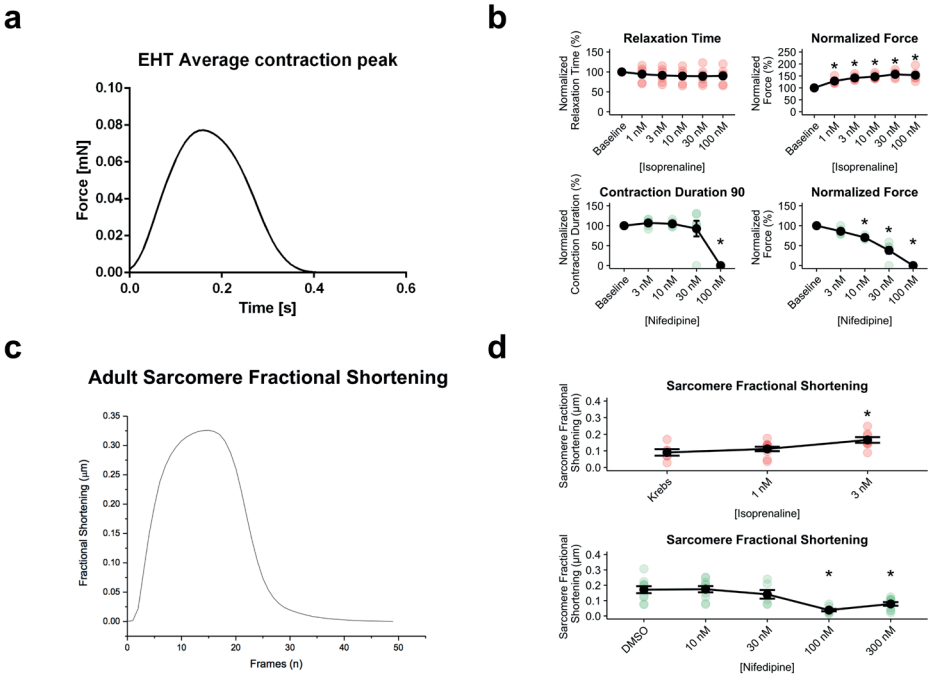

Supplementary Figure 6: Results from EHT and Adult gold standards

a) Representative average contraction profile obtained by pole deflection analysis of a single EHT during the recording period; b) average dose-response curves (black traces) and single measurements for several parameters obtained in EHTs treated with isoprenaline (top, red) and nifedipine (bottom, green) by pole deflection analysis; c) representative contraction profile obtained by sarcomere fractional shortening analysis of an adult rabbit CM; d) average dose-response curves (black traces) and single measurements for sarcomere fractional shortening obtained in adult CMs treated with isoprenaline (top, red) and nifedipine (bottom, green).

P-values baseline versus dose. Panel b i) 1 nM: 1; 3 nM: 1; 10 nM: 1; 30 nM: 1; 100 nM: 1. Panel b ii) 1 nM: 0.01517; 3 nM: 0.00016; 10 nM: $2.8 \cdot 10^{-5}$; 30 nM: $8.8 \cdot 10^{-7}$; 100 nM: $2.9 \cdot 10^{-6}$. (N=6; 6; 6; 6; 6; 6). Panel b iii) 3 nM: 1; 10 nM: 1; 30 nM: 1; 100 nM: $3.8 \cdot 10^{-7}$. Panel b iv) 3 nM: 0.2095; 10 nM: 0.0002; 30 nM: $5.2 \cdot 10^{-10}$; 100 nM: $1.2 \cdot 10^{-14}$. (N=6; 6; 6; 6; 6). Panel d i) 1 nM: 1; 3 nM: 0.018. Panel d ii) 10 nM: 1; 30 nM: 1; 100 nM: 0.00013; 300 nM: 0.00676.

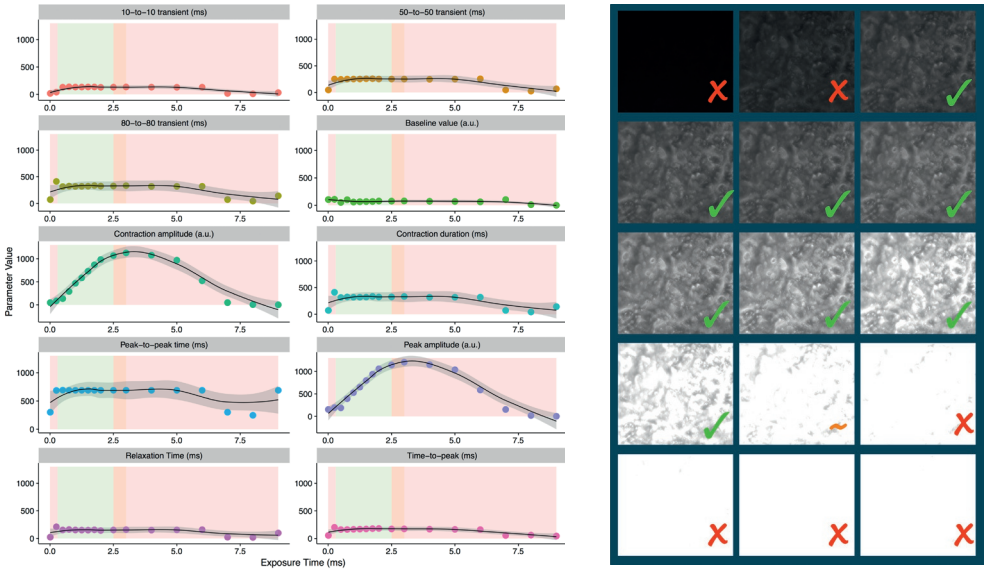

Supplementary Figure 7: MUSCLEMOTION behaviour with different camera exposures.

The output parameters of MUSCLEMOTION are shown for the same monolayer sample recordings with different exposure times. The contraction amplitude output increases linearly with increased exposure time while all temporal output parameters are independent of the lighting conditions within a reasonable range (i.e. the image should not be dark and it should not be saturated completely).

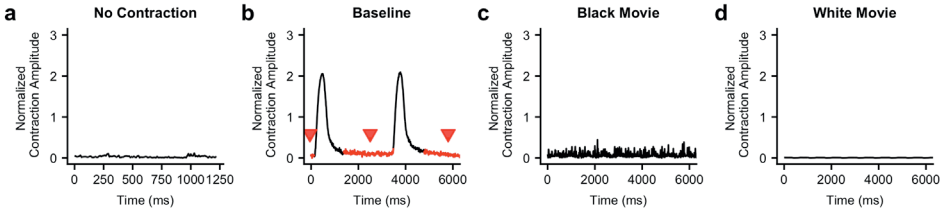

Supplementary Figure 8: Negative controls of MUSCLEMOTION.

The response of MUSCLEMOTION to a) a video of a single cell hPSC-CM that does not contract; b) a video of a contracting single cell hPSC-CM with baseline (i.e. diastolic period without contraction) indicated; c) a movie with extremely low exposure (i.e. black frames) and d) extremely high exposure (i.e. white frames).